SCIENTIFIC REPORTS

OPEN

Building better lithium-sulfur batteries: from $LiNO_3$ to solid oxide catalyst

Received: 10 June 2016
Accepted: 17 August 2016
Published: 15 September 2016

Ning Ding[1], Lan Zhou[1,2], Changwei Zhou[1], Dongsheng Geng[1], Jin Yang[1], Sheau Wei Chien[1], Zhaolin Liu[1], Man-Fai Ng[3], Aishui Yu[2], T. S. Andy Hor[1,4], Michael B. Sullivan[3] & Yun Zong[1]

Lithium nitrate ($LiNO_3$) is known as an important electrolyte additive in lithium-sulfur (Li-S) batteries. The prevailing understanding is that $LiNO_3$ reacts with metallic lithium anode to form a passivation layer which suppresses redox shuttles of lithium polysulfides, enabling good rechargeability of Li-S batteries. However, this view is seeing more challenges in the recent studies, and above all, the inability of inhibiting polysulfide reduction on Li anode. A closely related issue is the progressive reduction of $LiNO_3$ on Li anode which elevates internal resistance of the cell and compromises its cycling stability. Herein, we systematically investigated the function of $LiNO_3$ in redox-shuttle suppression, and propose the suppression as a result of catalyzed oxidation of polysulfides to sulfur by nitrate anions on or in the proximity of the electrode surface upon cell charging. This hypothesis is supported by both density functional theory calculations and the nitrate anions-suppressed self-discharge rate in Li-S cells. The catalytic mechanism is further validated by the use of ruthenium oxide (RuO_2, a good oxygen evolution catalyst) on cathode, which equips the $LiNO_3$-free cell with higher capacity and improved capacity retention over 400 cycles.

With high energy density and low cost, lithium-sulfur (Li-S) batteries are considered among the most promising candidates for next-generation energy storage devices[1–3]. The history of Li-S battery research dates back to 1960s[4], with most of the early works (1960–1990s) in primary batteries focusing on electrolyte optimization and sulfur utilization improvement[5]. The early research on the rechargeable ones, however, encountered the serious issue of fast capacity decay with very limited number of cycles (<20)[6–9]. The main cause of the poor rechargeability has been known as lithium polysulfide redox shuttles (LiPSs, soluble intermediates in charge/discharge reactions), which internally short-circuit the battery and display an ultra-long voltage plateau at ~2.35 V on charging[10]. Tricks were employed to rectify the cycling behavior by fixing the charge time in each subsequent cycle, which however led to partial charging with little improvement to the fast capacity decay of the batteries[6]. In addition, LiPSs redox shuttle was also found responsible for high self-discharge rate, warranting the urgency of research need in the development of high-performance Li-S batteries[11].

In 2008, Mikhaylik revealed the efficacy of $LiNO_3$ in suppressing LiPSs redox shuttles as a big breakthrough, enabling a real rechargeable Li-S battery with a coulombic efficiency (CE) of close to 100%[12]. Coincidentally, the introduction of $LiNO_3$ was found to concurrently improve the sulfur utilization rate in the cathode[13]. These promising results have made $LiNO_3$ the most important electrolyte additive and almost appear in every reported Li-S cell thereafter[14–18]. The function of $LiNO_3$, according to the prevailing understanding, is to form an electrically insulating layer on Li anode via a spontaneous reduction reaction which prevents further reduction of polysulfides thereon[19]. The passivation layer was identified as Li_xNO_y by Aurbach *et al.* using Fourier transform infrared (FTIR) spectroscopy and X-ray photoelectron spectroscopy (XPS)[13]. Later, Wen and co-workers reported $LiNO_3$-induced formation of smooth and dense solid electrolyte interphase (SEI) layer on Li anode[20], serving as

[1]Institute of Materials Research and Engineering (IMRE), A*STAR (Agency for Science, Technology and Research), 2 Fusionopolis Way, Innovis #08-03, Singapore 138634, Republic of Singapore. [2]Department of Chemistry, Shanghai Key Laboratory of Molecular Catalysis and Innovative Materials, Institute of New Energy, Fudan University, Shanghai 200438, P.R. China. [3]Institute of High Performance Computing (IHPC), A*STAR (Agency for Science, Technology and Research), 1 Fusionopolis Way, Connexis #16-16, Singapore 138632, Republic of Singapore. [4]Department of Chemistry, National University of Singapore, 3 Science Drive 3, Singapore 117543, Republic of Singapore. Correspondence and requests for materials should be addressed to Z.L. (email: zl-liu@imre.a-star.edu.sg) or M.-F.N. (email: ngmf@ihpc.a-star.edu.sg) or Y.Z. (email: y-zong@imre.a-star.edu.sg)

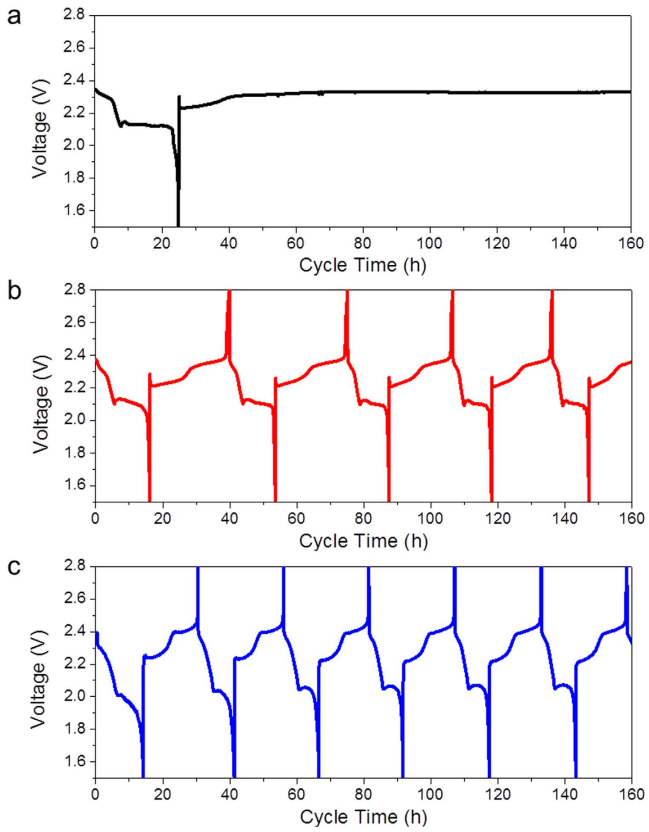

Figure 1. Temperature effect on the galvanostatic discharge-charge voltage profiles of sulfur-graphite composite cycled in $LiNO_3$-free electrolyte. The cell was tested at the temperature of 60 °C (**a**), room temperature (**b**) and −10 °C (**c**). At higher temperature the shuttle phenomenon became more distinct.

a protection layer to the reductive Li metal[21]. Inspired by these promising results, significantly more efforts were devoted to rechargeable Li-S battery research on nanostructured sulfur cathode development, leading to the revelation of a large number of interesting materials and findings[22–26]. Nevertheless, recent work of K. Amine's group showed the irrelevance of redox shuttle suppression to the Li_xNO_y layer[27], triggering new thinking on future Li-S battery development. Another related phenomenon that echoes this argument is the finding of progressive $LiNO_3$ reduction on Li anode, which suggests the ineffectiveness of a Li_xNO_y layer in prevention of LiPSs reduction[28]. All these unambiguously justified the necessity of relooking into the role of $LiNO_3$ in rechargeable Li-S batteries. Herein, we revisit some key factors that influence LiPSs redox shuttles, clarify the roles of Li_xNO_y passivation layers, and propose a new mechanism that redox shuttle suppression in the presence of $LiNO_3$ is due to the strong binding between the soluble high-order LiPSs and nitrate (NO_3^-) anions adsorbed on carbon substrate, which promotes the oxidation of polysulfide to sulfur on charging. This is supported by density functional theory (DFT) calculations and NO_3^--induced low self-discharge rate in Li-S batteries. As the progressive reduction of $LiNO_3$ compromises long-term cycling stability of Li-S batteries by gradual increase of the internal resistance, we propose the substitution of soluble $LiNO_3$ with solid oxide catalyst of good polysulfide oxidation reaction (PSOR) activity, to which ruthenium oxide was found as a preferable choice.

Results and Discussion

Rationale of experimental conditions. Initial coulombic efficiency (ICE) of a rechargeable battery reflects the reversibility of its cell reactions in the first cycle and is typically above 90% for commercial Li-ion batteries. In a Li-S battery with $LiNO_3$-free electrolyte, ICE varies notably due to the different extent of redox shuttles. To clarify the role of $LiNO_3$, general factors that influence ICE must be fixed, e.g. Li salts concentration and applied current[29], in all cells are 1 M LiTFSI in DOL/DME (v/v, 1:1) and 0.1 mA, respectively.

In addition, sulfur loading density (SLD) was found to affect ICE (Fig. S1, Supplementary Information). At SLD $<0.8\,mg\,cm^{-2}$, ICE experienced a quasi-linear decrease with the increase of SLD; whereas at SLD $>1.1\,mg\,cm^{-2}$, increase of SLD elevates ICE slowly. Interestingly, at $0.8 < SLD < 1.1\,mg\,cm^{-2}$ ICE exhibits a buffer-like behavior and fluctuates at $62 \pm 5\%$. This unique feature is ideal for the study of redox shuttle effect, as the effect of SLD to ICE can be neglected if it is fixed at $0.9 \pm 0.1\,mg\,cm^{-2}$.

Moreover, the volume of electrolyte shows a direct impact on ICE (Fig. S2, Supplementary Information). On a Li-S cell with 80 μL of electrolyte, an ultra-long charge voltage plateau at 2.35 V presents with an ICE of 66.4%. In contrast, as the electrolyte was reduced to 10 μL, a similar cell delivers a decent cycling performance with an ICE as high as

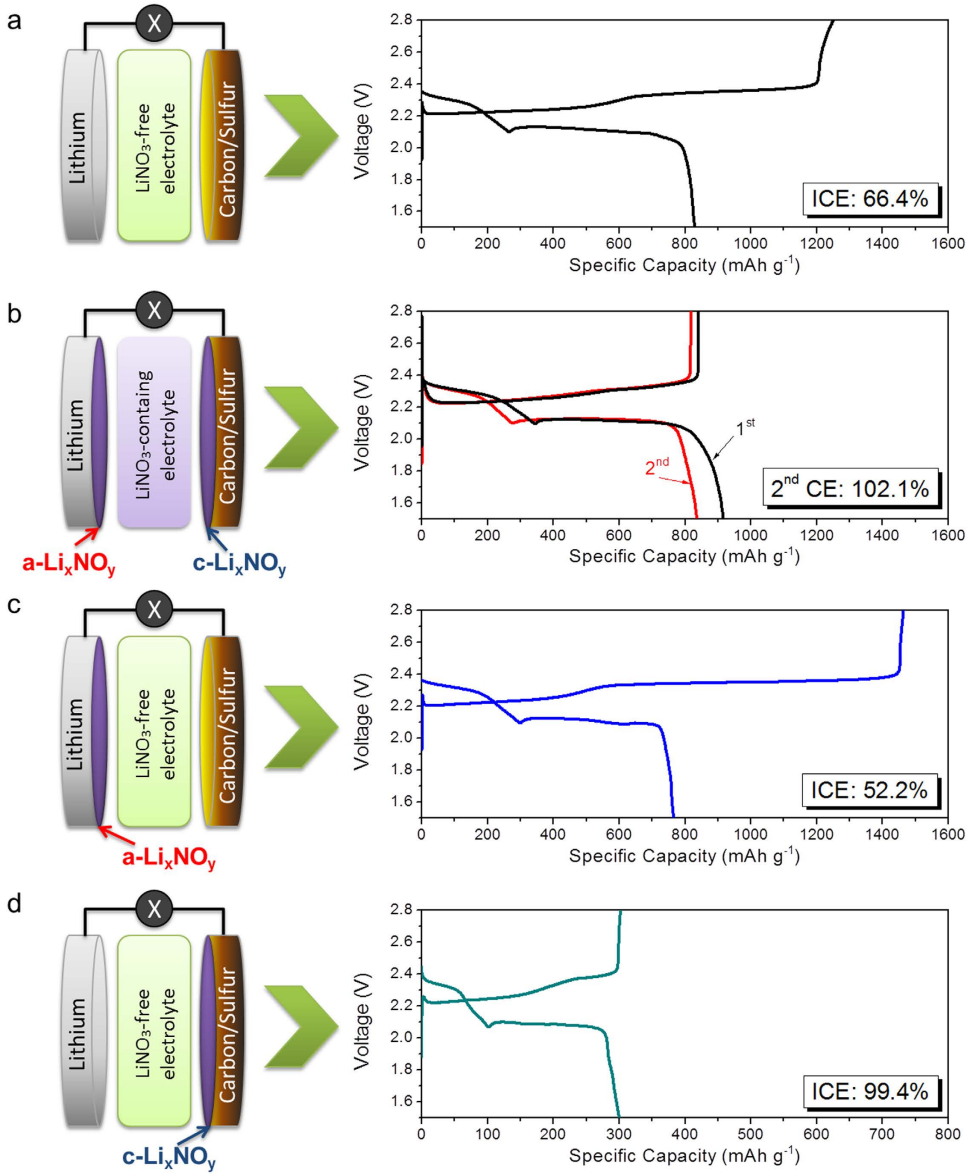

Figure 2. Galvanostatic discharge-charge voltage profiles of Li-S batteries (with sulfur-graphite composite). (**a**) 1st cycle of a Li-S cell cycled in $LiNO_3$-free electrolyte, with an ICE of 66.4% as the benchmark. (**b**) The 2 cycles of the cell cycled in $LiNO_3$-contained electrolyte which was later dissembled to obtained Li_xNO_y coated Li anode and carbon/sulfur cathode. The reduction of $LiNO_3$ on cathode leads to a CE value of ~100%. Li_xNO_y passivation layers formed on both sides of electrodes, assigned to a-Li_xNO_y for anode side and c-Li_xNO_y for cathode side, respectively. (**c**) The first cycle of the reassembled cell from the used Li anode (with a-Li_xNO_y surface coating) and a fresh carbon/sulfur cathode in $LiNO_3$-free electrolyte, showing an ICE of 52.2%. (**d**) The first cycle of the reassembled cell with a fresh Li anode and the used carbon/sulfur cathode (with c-Li_xNO_y surface coating) in $LiNO_3$-free electrolyte, giving an ICE of 99.4%.

99.1%. The notably higher ICE at smaller volume of electrolyte was likely due to the increased viscosity of electrolyte at much higher LiPSs concentration that slowed down the diffusion of LiPSs from cathode to anode. This was supported by the "recovered" low CE when the cell was given sufficient time for relaxation between charges (Fig. S3, Supplementary Information). The electrolyte volume effect to the cycling performance of Li-S cells can be found in a systematic study by Zhang[30], showing the importance of electrolyte volume optimization to the high performance cells. In this study, we fixed the electrolyte volume as 80 μL in cells for ICE study, and 30 μL in those for cycling/storage tests.

Further, ICE varies with the change of the operating temperature of the cells (Fig. 1). At a higher temperature, e.g. 60 °C, the severe redox shuttles internally short-circuited the Li-S cell, leading to "infinite" charging; whereas at an operating temperature of −10 °C, ICE of 84.9% was achieved with redox shuttling phenomenon hardly visible. At conventional operating temperature, i.e. room temperature of 25 °C, a Li-S cell with 80 μL electrolyte and SLD of 0.9 mg cm^{-2} delivers ICE of 66.4%. Such cells with moderate ICE values are ideal for the

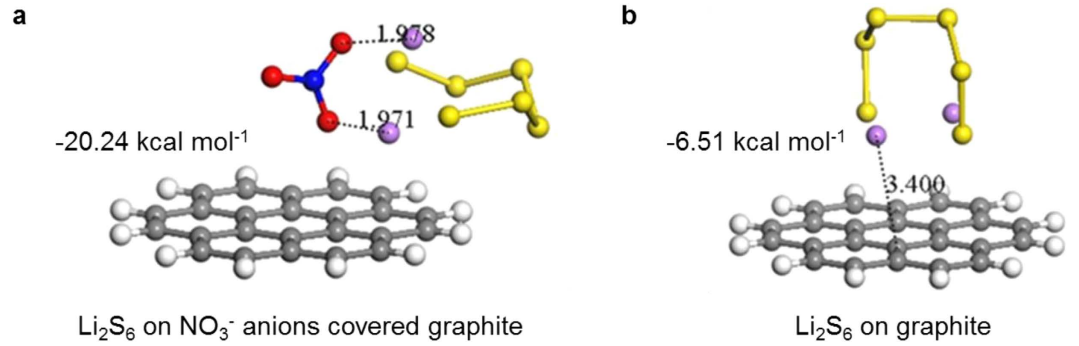

Figure 3. Optimized structures of Li_2S_6 on NO_3 covered graphite and pure graphite models, and the corresponding adsorption energies. (**a**) Li_2S_6 on NO_3^- covered graphite; (**b**) Li_2S_6 on graphite. Red, blue, yellow, purple, grey and white balls represent O, N, S, Li, C and H atoms, respectively. The numbers indicate the bond lengths in Å.

clarification on the role and efficacy of $LiNO_3$ additive in Li-S batteries. All experiments were thus conducted at room temperature unless stated otherwise.

Inability of Li_xNO_y layers on electrodes in redox shuttle suppression. To re-evaluate the efficacy of a Li_xNO_y passivation layer in redox shuttle suppression, we constructed 3 types of Li-S cells, i.e. with Li_xNO_y passivation layer only on anode or cathode, or absent on both electrodes, and get them cycled in $LiNO_3$-free electrolyte, respectively. The results show that in the absence of $LiNO_3$ and Li_xNO_y passivation layer, a Li-S cell delivers a reproducible initial coulombic efficiency (ICE) of 66.4% (Fig. 2a). At this ICE the LiPSs redox shuttle phenomenon is severe and reflected as an abnormally high charge capacity (or "infinite charging"). In contrast, a replicate cell cycled in $LiNO_3$-contained electrolyte gave a reversible efficiency of ~100% in 2nd cycle (Fig. 2b), showing the efficacy of $LiNO_3$ in electrolyte for redox-shuttle suppression. The overshoot of ICE above a unit in the 1st cycle (and slightly in the 2nd cycle) was due to the side reaction of $LiNO_3$ reduction on cathode (forming Li_xNO_y layer) at the voltage below 1.85 V (Fig. S4, Supplementary Information).

As a "used" Li-S cell with Li_xNO_y layers on both electrodes was disassembled at full-charge state (2.8 V) in an Ar-filled glove box, *a*-Li_xNO_y protected anode and *c*-Li_xNO_y covered cathode were collected (*a* and *c* here stand for anode and cathode, respectively). After cleansed using fresh electrolyte solvent, the *a*-Li_xNO_y/Li anode was coupled with a new carbon/sulfur cathode to form a new Li-S cell in $LiNO_3$-free electrolyte (Fig. 2c). Surprisingly, with a discharge capacity of 765 mAh g^{-1} the cell showed a charge capacity of 1464 mAh g^{-1}, which corresponds to an ICE of as low as 52.2%. This result suggests the inability of *a*-Li_xNO_y layer in LiPSs redox shuttle suppression, echoing the previous report of Amine *et al.*[27].

Interestingly, a Li-S cell assembled using the cleansed *c*-Li_xNO_y covered cathode and a fresh Li anode in $LiNO_3$-free electrolyte was able to deliver an ICE of 99.4% (Fig. 2d), indicating excellent redox-shuttle suppression. Nevertheless, a notable drop in the cell capacity (300 *vs.* 765 mAh g^{-1}) is likely due to the dissolution of sulfur/LiPSs into the electrolyte in the previous cell during the preparation of *c*-Li_xNO_y covered cathode. This was supported by a higher capacity retention (511 mAh g^{-1}) when the electrolyte volume was reduced from 80 to 30 μL. It is worth noting that this high ICE does not necessarily originate from the *c*-Li_xNO_y layer. The *c*-Li_xNO_y covered cathode with a rough surface was difficult to be fully cleansed, leaving $LiNO_3$ residues on (or in the proximity of) the cathode surface or inside the binder polymer matrix which works in its own way to suppress the redox shuttles.

The necessity of *c*-Li_xNO_y for high ICE was further excluded by cycling a freshly assembled Li-S cell of Li anode and carbon/sulfur cathode in $LiNO_3$-contained electrolyte with a cut-off voltage of 2.0 V, whereby the reduction of $LiNO_3$ on cathode unlikely took place and hence a *c*-Li_xNO_y layer was absent[31]. Nonetheless, the ICE value was found as high as that of the cell discharged to 1.5 V with the formation of *c*-Li_xNO_y (Fig. S5, Supplementary Information). Similar experiment has also been carried out by Zhang recently and NO_3 radical intermediate was proposed as the key in shuttle suppression[32]. In our experiment, $LiNO_3$ was replaced by $NaNO_3$ in the electrolyte (Fig. S6, Supplementary Information) and a high ICE was also obtainable. These results have clearly suggested that instead of *c*-Li_xNO_y, it was NO_3^- anions adsorbed on (or in the proximity of) cathode suppressing the redox shuttles.

Stronger binding of LiPSs to NO_3^--theoretical calculations and self-discharge test. A possible mechanism for redox shuttle suppression by NO_3^- anions on (or in the proximity of) the graphitic electrode surface is that these anions promote/catalyse a faster oxidation of soluble high-order LiPSs into element sulfur on charging such that fewer LiPSs diffuse to anode surface to undergo a reduction reaction. At higher charge voltage (2.35 V plateau) the redox shuttle phenomenon is a competing process with the oxidation of $Li_2S_4 \rightarrow Li_2S_6 \rightarrow Li_2S_8 \rightarrow S_8$. With Li_2S_6 as the most stable LiPS[33], a stronger binding of Li_2S_6 to NO_3^- anions on (or in the proximity of) graphite than directly to C atoms of graphite would support the proposed oxidation mechanism[34]. Hence, we calculated the adsorption energies of Li_2S_6 onto NO_3^- anions covered graphite and onto

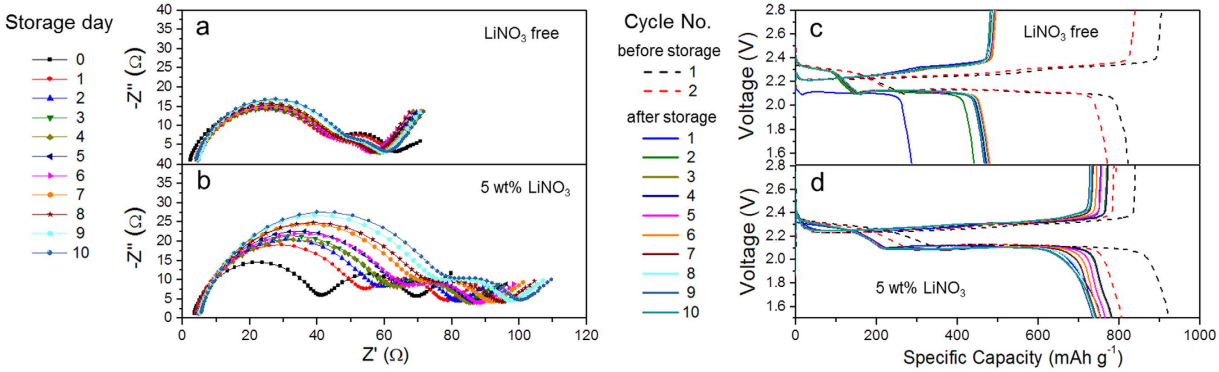

Figure 4. Self-discharge test of Li-S batteries (with sulfur-graphite composite). Nyquist plots and capacity change of the cells with no $LiNO_3$ (**a,c**), 5.0 wt% of $LiNO_3$ (**b,d**) stored at room temperature over 10 days. Electrolyte volume: 30 μL.

pure graphite in electrolyte solvent, respectively. The density functional theory (DFT) modelling data (Fig. 3) shows that on NO_3^- anions covered graphite Li atoms in Li_2S_6 "bond" to O atoms in NO_3^- with a "bond-length" of 1.978 or 1.971 Å, comparable to a typical N−H hydrogen bond (1.97 Å). In contrast, on pure graphite Li atoms interacted to C atoms. The Li−C distance in this case was 3.400 Å, which came to the edge of distance for dispersive interaction. Clearly, it has suggested much stronger Li−O interactions between Li and O of NO_3^- than Li−C interactions between Li and C of graphite. This is further supported by the larger adsorption energy for Li_2S_6 on NO_3^- (−20.24 kcal mol^{-1}) than that on pure graphite (−6.51 kcal mol^{-1}). Similar scenario has also been reported previously by Wang *et al.* in a study of graphene oxides[35]. Such notably strong binding can be seen as the first step of the proposed catalytic mechanism. Since it was known that LiPSs→sulfur conversion on pure carbon was hardly possible in the absence of $LiNO_3$[36,37], the strong LiPSs/NO_3^- bonding enabled oxidation conversion of polysulfides on cathode upon charging of the battery could be seen as a catalytic process.

The strong LiPSs/NO_3^- interaction should also help suppress the reduction of S_8 to Li_2S_6 for storage, which is reflected as lower self-discharge rate in battery. This was proven by monitoring the impedance changes of a fully-charged Li-S cell with electrolyte containing 5.0 wt% of $LiNO_3$ over 10 days of storage at room temperature, using its $LiNO_3$-free counterpart as the control (Fig. 4a,b). In the Nyquist plot the first semi-circle at high frequency range was attributed to the resistance of solid electrolyte interface (R_{SEI}), whereas the second one at middle frequency range was ascribed to the charge transfer (R_{ct}). The simulation data shows that for the cell with $LiNO_3$-contained electrolyte R_{SEI} increased from 37.2 to 70.1 Ω over 10 days (Fig. S7, Supplementary Information), which was notably higher than that of its $LiNO_3$-free counterpart (from 38.8 to 42.3 Ω). Fast increase of R_{SEI} in the presence of $LiNO_3$ electrolyte additive is attributed to progressive reduction of $LiNO_3$ on Li anode[29]. Here, the drop of R_{ct} is more of a concern, as it reflects the state-of-charge of a cell[31]. R_{ct} is larger for higher charged state, and its sharper decrease indicates faster self-discharge. Thus, the slower drop of R_{ct} (27.1 → 24.0 Ω, or 3.1 Ω) for the cell with $LiNO_3$-contained electrolyte as compared to that of its $LiNO_3$-free counterpart (22.8 → 12.8 Ω, or 10.0 Ω) is suggesting the clear inhibition of self-discharge by $LiNO_3$. This is understandable, as NO_3^- anions covered graphite were able to hold LiPSs more tightly and thus notably slowed down the self-discharge process (S_8 → LiPSs).

The inhibited self-discharge in cells with $LiNO_3$-contained electrolyte was echoed by its higher open circuit voltage (OCV, 2.33 V) after 10 days of aging at room temperature as compared to that of the $LiNO_3$-free counterpart (2.16 V, Fig. S8, Supplementary Information). The self-discharge suppression is achieved through the strong interactions between Li and O of NO_3^- anions covered graphite and irrelevant to the presence of the *c*-Li_xNO_y layer on cathode, evidenced by a similar OCV when setting a higher cut-off voltage (2.0 V). In cells with $LiNO_3$-free electrolyte, self-discharge over time led to the disappearance of the upper voltage plateau corresponding to the series reductions of $S_8 \rightarrow Li_2S_8 \rightarrow Li_2S_6 \rightarrow Li_2S_4$ in the following discharge (Fig. 4c). As LiPSs in electrolyte can diffuse to the surface of Li anode and eventually precipitate thereon in the form of solid Li_2S/Li_2S_2[13], irreversible capacity decay was seen with only 61.5% of capacity retention after the storage of 10 days (475 *vs.* 772 mAh g^{-1}). In sharp contrast, cells with $LiNO_3$-contained electrolyte were able to retain 97.0% of capacity (783 *vs.* 807 mAh g^{-1}) over the same period (Fig. 4d). The significantly suppressed self-discharge in the presence of $LiNO_3$ provides a solid support to the stronger interaction of NO_3^- anions on graphite to LiPSs (Li_2S_6) in Li−O "bonding" mode. This further supported the catalytic mechanism of redox-shuttle suppression by $LiNO_3$.

Despite its high efficacy on LiPSs redox shuttle suppression and self-discharge mitigation, use of $LiNO_3$ in electrolyte brings in two noticeable drawbacks to the cycling stability of Li-S cells. One is the progressive reduction of $LiNO_3$ on Li anode, elevating cell internal resistance which lowers the discharge voltage[28]; the other is the formation of Li_xNO_y passivation layer on cathode at low voltage which destabilizes the cathode upon charging and induces faster capacity decay[31,38]. It is worth noting that cells with $LiNO_3$ in electrolyte are generally in a non-equilibrium state, whereby the free $LiNO_3$ will be gradually depleted by continuous reduction on both electrodes. Eventually NO_3^- anions on (or in the proximity of) graphite will diffuse into the electrolyte and get consumed as well. This is evidenced by the clear decrease of CE in long-term cycling test of cells using

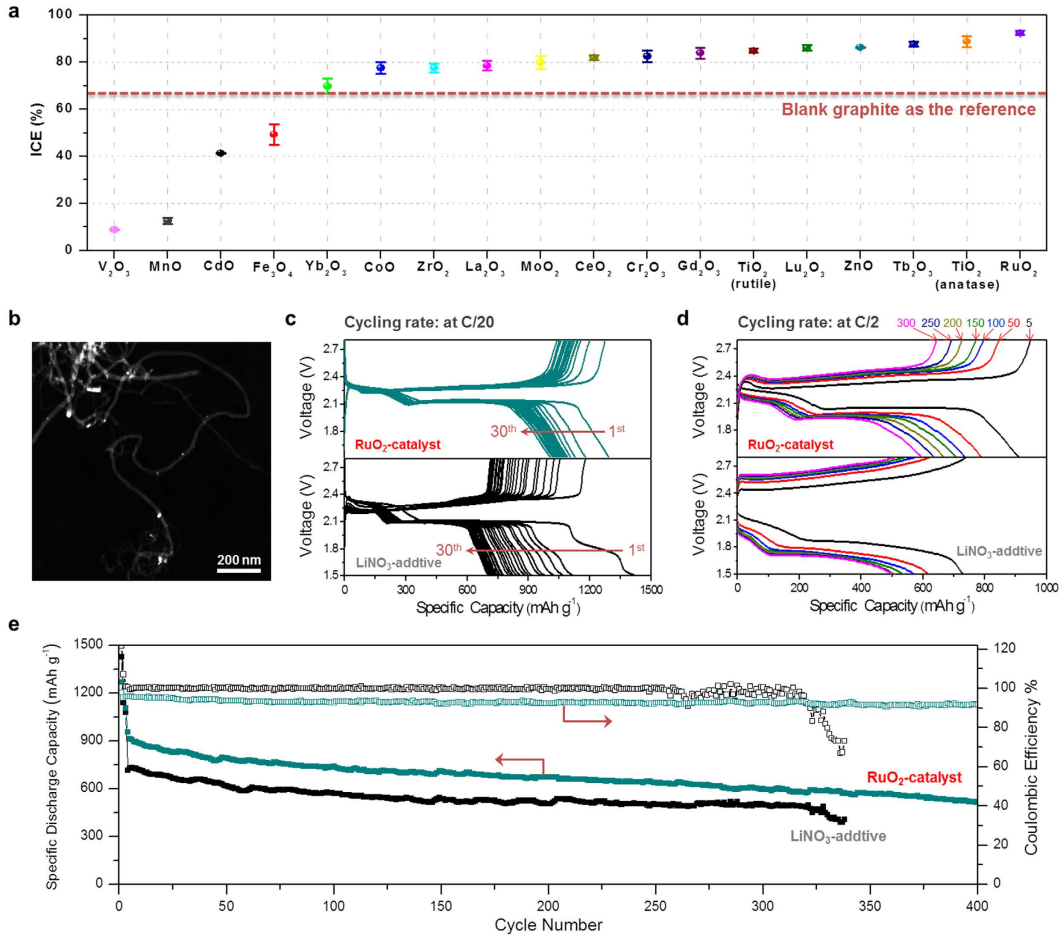

Figure 5. (**a**) ICE data of the Li-S cells with the introduction of different transition metal oxides on graphite substrate. (**b**) HAADF-STEM image of RuO_2-MWCNTs composite. (**c,d**) Galvanostatic discharge-charge voltage profiles of the cell with RuO_2 catalyst cycled in $LiNO_3$-free electrolyte (top) and the bared MWCNTs-sulfur electrode cycled in the electrolyte with 2.0 wt% of $LiNO_3$ additive (bottom) at the cycling rate of C/20 (from 1st to 30th cycle) and C/2 (in 5th, 50th, 100th, 150th, 200th, 250th and 300th cycle). (**e**) Comparison of the cycling performance of the cell with RuO_2 catalyst and that with $LiNO_3$ additive (at C/2). The cells were first stabilized at C/20 for 3 times.

$LiNO_3$-contained electrolyte in previous studies[16,39–41]. Searching of a replacement for $LiNO_3$ becomes necessary for Li-S batteries with long-term cycling stability.

Replacing $LiNO_3$ with transition metal oxides. Different from Zhang's proposal of NO_3 radical intermediate as the key to promote LiPSs→sulfur conversion[32], we believe that the shuttle suppression could be achieved by incorporating solid transition metal oxides into cathode as a catalyst of polysulfide oxidation reactions (PSOR). Some transition metal oxides were employed previously as polysulfide absorbents to improve the performance of Li-S cells, with Magnéli-phase Ti_4O_7 being a successful example[42,43]. Moreover, MnO_2[44], ZrO_2[45], La_2O_3[46], $NiFe_2O_4$[47] and $Ni_3(NO_3)_2(OH)_4$[48] as a major component in cathode, were found to improve the Li-S cell performances in different ways. The new understanding on the role of $LiNO_3$ in this work makes us believe that transition metal oxides may be used in low content to "catalyze" the oxidation of the adsorbed polysulfide, if their interactions are strong. To validate this catalytic mechanism, we introduced low content (<3 wt% in the sulfur electrode) of transition metal oxides (18 in total) to investigate their activities towards PSOR. In each experiment one of the 18 transition metal oxides, selected from Period 4 (Fig. S9, Supplementary Information), 5 (Fig. S10, Supplementary Information), and rare earth elements in the lanthanide series (Fig. S11, Supplementary Information) of the periodic table, was loaded onto graphite. The composition and structure of these graphite/oxide composites were confirmed by their respective X-ray diffraction (XRD) patterns (Fig. S12, Supplementary Information). After mixing with sulfur to form the cathode, the shuttle effect of LiPSs in the obtained Li-S cell was studied. The ICE data (Fig. 5a) clearly shows that V_2O_3, MnO, CdO and Fe_3O_4 imposed a negative effect on ICE (<50%), whereas anatase-TiO_2, rutile-TiO_2, Cr_2O_3, ZnO, RuO_2 and most rare earth oxides improved the ICE (>80%) as compared to bare graphite (ICE: 66.4%). It is noteworthy that a direct correlation between CE value and different transition metal oxide here would be hardly achievable. Their binding affinity to polysulfides could be an important factor which, however, is extremely difficult to be accurately quantified due

to various complications, e.g. crystal phase, dominating surface atoms, orientation, overall exposure to surface of electrode made from slurry method, etc. These factors could vary notably for different metal oxide species. One point to note could be the adverse impact of V_2O_3 and MnO with notable reduction power, which may compete with the "polysulfide oxidation reaction" and make the latter more difficult to take place. A clearer picture may be available after more discrete research on various transition metal oxides are studies in great details in future.

Coincidentally, RuO_2, an efficient catalyst towards oxygen evolution reaction (OER)[49], was found to be the most effective catalyst towards PSOR among these oxides, furnishing Li-S cells with the highest CE (92.5%) and superior cycling stability as compared to their $LiNO_3$-based counterparts (Fig. 5b–d). The discharge capacity can be improved by replacing graphite (17.8 m^2 g^{-1}, Fig. S13, Supplementary Information) with large surface area carbon, e.g. multi-walled carbon nanotubes (MWCNTs, 256.3 m^2 g^{-1}). Figure 5b shows the high-angle annular dark-field scanning transmission electron microscopy (HAADF-STEM) image of MWCNTs decorated with RuO_2 and the bright dots indicate the location of well-dispersed RuO_2 nanoparticles. By employing a cathode of MWCNTs/sulfur composite with 2.87 wt% RuO_2, initial discharge capacity of as high as 1298 mAh g^{-1} was achieved at a current density of C/20 (1C = 1672 mAh g^{-1}, Fig. 5c). In contrast, the MWCNTs/sulfur composite based Li-S cells without RuO_2 gave additional two potential plateaus at lower voltages (<1.89 V, Fig. S14, Supplementary Information), attributing to the reduction of $LiNO_3$ which is detrimental to the long-term cycling stability of the cell. One may eliminate $LiNO_3$ reduction at cathode side by setting a higher cut-off voltage, as suggested by Aurbach[38]; however, the progressive $LiNO_3$ reduction on Li anode remains an issue[28]. It is hence not surprising to see faster capacity fading in cells cycled in $LiNO_3$-contained electrolyte than in the ones with RuO_2 as a replacement (Figs 5c and S15, Supplementary Information). The improvement of battery performance becomes more pronounced at elevated cycling rate (C/2), reflected as higher capacity and smaller voltage gap (Fig. 5d). For instance, in 5th cycle the cell with RuO_2 delivers a discharge capacity of 912.4 mAh g^{-1}, which is notably higher than the one with $LiNO_3$ additive (729.8 mAh g^{-1}). Meanwhile, the much smaller voltage gap (0.266 *vs.* 0.686 V, in 5th cycle at a discharge capacity of 400 mAh g^{-1}) corresponds to a higher round-trip efficiency of the cell equipped with RuO_2 (84.1 *vs.* 61.6%). The lower discharge voltage at higher rate for battery using $LiNO_3$ additive was likely due to the higher impedance caused by the introduction of Li_xNO_y layer as a result of $LiNO_3$ reduction. This again shows the advantage of using transition metal oxide, whereby the Li_xNO_y layer formation can be avoided. In a long-cycling test for batteries with transition metal oxide or $LiNO_3$, similar capacity fading trends were observed for both cells in the first 250 cycles except higher capacity for the former in the same cycle. The similar fading trend was likely due to the loss (with cycling) of active materials (sulfur) on cathode which still remains an issue to be solved. The lower capacity (retention) at C/2 for the one with $LiNO_3$ additive was due to its higher impedance from the Li_xNO_y layers as we discussed before. Adverse effect rising from the $LiNO_3$ progressive reduction started to become more prominent from 250 cycles, and the cells become unstable as clearly evidenced by the oscillated CE values (Fig. 5e). The same phenomenon is also observed in Li-S cells with graphite/sulfur electrodes (Fig. S16, Supplementary Information) and also a recent study by Janek *et al.*[50]. Interestingly, a Li-S cell with RuO_2 on cathode exhibited a constant CE and was able to deliver a discharge capacity of 513.3 mAh g^{-1} (@C/2) even after 400 cycles.

Conclusion

In summary, we re-examined the efficacy of Li_xNO_y layers on both anode and cathode in redox shuttle suppression, and found both ineffective. Previously observed convincing phenomenon of redox shuttle suppression by $LiNO_3$ additive in electrolyte could have functioned through the NO_3^- anions on or in the proximity of the graphitic surface in sulfur cathode. These anions bind strongly to LiPSs via "bond-like" interaction, facilitating fast LiPSs→sulfur conversion which mitigates the diffusion of LiPSs to anode in charge process. The stronger binding was confirmed by DFT calculations and echoed by $LiNO_3$-enabled low self-discharge rate in Li-S batteries. To replace $LiNO_3$ for long-term cycling stability, low content insoluble solid transition metal oxide was incorporated into carbon substrate in sulfur cathode. RuO_2, a prominent OER catalyst, enables an ICE of 92.5% with improved long-term cycling stability. This work opens a new research path for the development of Li-S batteries, i.e. using polysulfide oxidation catalysts as enablers to realize long-term cycling stability.

Methods

Materials and electrochemical characterizations. Primary synthetic graphite (TIMCAL TIMREX® KS6), multi-walled carbon nanotubes (MWCNTs, Aldrich, O.D. × L: 6–9 nm × 5 μm, purity: >95%), precipitated sulfur powder (Alfa Aesar, 99.5%) and poly(vinylidenefluoride) (PVDF, Solef® 5130) were used as received. The graphite/sulfur cathode was prepared by manually mixing graphite and sulfur (w/w, 1:1) in an agate mortar to form a graphite/sulfur composite which was then formulated to a slurry with PVDF in 1-methyl-2-pyrrolidinone (NMP, anhydrous, Aldrich) (w/w: 95/5), and cast evenly onto a piece of aluminum (Al) foil. For the CNT/sulfur cathode, PVDF content was increased to 10 wt% to ensure strong adhesion of active material on Al foil. After drying in air at 80 °C for 2 h, electrode discs of 15 mm in diameter were punched out and transferred into an argon-filled glove box (MBraun) for assembly of Li-S cells. The electrolyte used was 1 M lithium bis(trifluoro-methanesulfonyl) imide (LiTFSI, Aldrich, 99.0%) in a solvent of 1,2-Dimethoxyethane (DME, Alfa Aesar, 99+%) and 1,3-Dioxolane (DOL, Alfa Aesar, 99.5%) (v/v, 1:1), or with additional 5.0 wt% of lithium nitrate ($LiNO_3$, Aldrich, 99.0%) as additive. The lithium salts were further dried at 150 °C for 15 h before transferring into the glove box.

The impregnation of RuO_2 was via co-precipitation method. 0.26 g of MWCNTs (or KS6 graphite) was first dispersed in a solvent (100 mL) of 2-propanol and acetone (v/v, 1:1) under sonication. Then ruthenium chloride ($RuCl_3 \cdot xH_2O$, Alfa Aesar) was dissolved in the above suspension. Subsequently, sodium hydroxide solution (0.1 g mol^{-1}, 12 mL) was slowly added with vigorous stirring at room temperature. The obtained composite was collected by centrifugation at 6,000 rpm, then thoroughly washed by deionized water until no chloride ions was

detected by silver nitrate solution, and finally dried at 180 °C for 15 h. The synthesized ruthenium compound was determined to be rutile RuO_2 (JCPDS #43-1027) by X-ray diffraction pattern (Bruker D8 Advance) and the loading on carbon is 6.38 wt% (or 2.87 wt% in RuO_2-MWCNTs-sulfur cathode), confirmed by thermogravimetric analysis (TGA, TA Instruments Q500). TEM image was collected from the monochromated transmission electron microscope (FEI, Titan) in a scanning mode. The RuO_2-MWCNTs-sulfur cathode is composed of 45 wt% of sulfur, 45 wt% of RuO_2-MWCNTs composite and 10 wt% of PVDF, with the sulfur loading density of 0.66 mg cm^{-2}. The RuO_2-graphite-sulfur cathode contains 47.5 wt% of sulfur, 47.5 wt% of RuO_2-graphite composite and 5 wt% of PVDF, with a typical sulfur loading density of ~0.9 mg cm^{-2}. The cells were cycled in the electrolyte containing 1 M LiTFSI in DME/DOL (v/v, 1:1), or with additional 2.0 wt% of $LiNO_3$ as additive.

Electrochemical performance was studied using CR2032-type coin cells with Li metal (diameter: 15.8 mm) counter electrode and Celgard 2400 separator. The cells were tested on a multichannel battery tester (Shenzhen Neware) at a constant current of 0.1 mA. The cycling voltage range was set between 1.5 and 2.8 V. To clarify the role of Li_xNO_y passivation layers, the Li-S cells were run over 3 cycles and disassembled at full-charge state (2.8 V) in a glove box. The obtained cycled electrodes were washed a few times using a mixture solvent of DME and DOL (v/v, 1:1, pre-treated by metallic lithium stripes over 48 h) before re-assembling into new cells with a fresh counter electrode and $LiNO_3$-free electrolyte. Electrochemical impedance spectra (EIS) were recorded on an Autolab instrument in the frequency range of 100 kHz to 50 mHz at room temperature. To amplify the self-discharge effect, the sulfur loading density (SLD) of the cells for storage test was reduced to 0.8 mg cm^{-2}.

Computational methods. A single layer of graphite (coronene structure) was adopted to represent the simplest cluster model of graphite, with Li_2S_6 as the most stable LiPSs being used in DFT calculations. The optimized Li_2S_6 exhibited a ring-like structure which resembles cyclo-octasulfur (S_8). The additive NO_3^- and Li_2S_6 placed above the plane of the graphite model were used as the starting geometry. Geometry optimization was performed using unrestricted wB97XD density functional in Gaussian 09 suite of program[51,52]. The selected functional uses Grimme's D2 empirical dispersion correction[53] that accounts for long-range interactions corrections. The 6-31+ G(d,p) basis sets were adopted for H, Li, C, N O and S atoms[54–56]. The selected basis sets contained diffuse functions which describes charged species. Self-consistency-field energy convergence was set at 10^{-6} Hartree. 1,2-dimethoxyethane (DME) is used as the solvent within the polarization continuum model (PCM)[57]. Four parameters are set for this solvent: the static dielectric constant (eps) = 7.2; the molecular radius of the solvent (rsolv) = 2.78255 Å; the density of the solvent (density) = 0.005804 particles $Å^{-1}$ and the molar volume of the solvent (vmol) = 103.7911 cm^{-3}. The rest are based on the default parameters of water solvent. Zero-point energy corrections obtained from vibrational frequency calculations in solvent are included in the adsorption energy (E_{ad}) calculations. E_{ad} is calculated using the formula:

$$E_{ad} = E_{additive/Li2S6/graphite} - (E_{additive/graphite} + E_{Li2S6}) \quad (1)$$

where $E_{additive/Li2S6/graphite}$, $E_{additive/graphite}$ and E_{Li2S6} are the total energy of optimized models of additive/Li_2S_6/graphite, additive/graphite, and Li_2S_6 polysulfide, respectively. The more negative adsorption energy indicates stronger binding strength.

References

1. Scrosati, B. & Garche, J. Lithium batteries: status, prospects and future. *J. Power Sources* **195,** 2419–2430 (2010).
2. Yin, Y.-X., Xin, S., Guo, Y.-G. & Wan, L.-J. Lithium-sulfur batteries: electrochemistry, materials, and prospects. *Angew. Chem. Int. Ed.* **52,** 13186–13200 (2013).
3. Bruce, P. G., Freunberger, S. A., Hardwick, L. J. & Tarascon, J.-M. Li-O_2 and Li-S batteries with high energy storage. *Nat. Mater.* **11,** 19–29 (2012).
4. Danuta, H. & Juliusz, U. inventors; Electric Techniques Corp., assignee. Electric dry cells and storage batteries. United States patent US 3,043,896. 1962 Jun 10.
5. Manthiram, A., Fu, Y., Chung, S.-H., Zu, C. & Su, Y.-S. Rechargeable lithium-sulfur batteries. *Chem. Rev.* **114,** 11751–11787 (2014).
6. Marmorstein, D. *et al.* Electrochemical performance of lithium/sulfur cells with three different polymer electrolytes. *J. Power Sources* **89,** 219–226 (2000).
7. Trofimov, B. A. *et al.* Vinyl ethers with polysulfide and hydroxyl functions and polymers therefrom as binders for lithium-sulfur batteries. *J. Appl. Polym. Sci.* **101,** 4051–4055 (2006).
8. Yuan, L. X. *et al.* Improved dischargeability and reversibility of sulfur cathode in a novel ionic liquid electrolyte. *Electrochem. Commun.* **8,** 610–614 (2006).
9. Wang, J. *et al.* Sulphur-polypyrrole composite positive electrode materials for rechargeable lithium batteries. *Electrochim. Acta* **51,** 4634–4638 (2006).
10. Wang, Q. *et al.* A shuttle effect free lithium sulfur battery based on a hybrid electrolyte. *Phys. Chem. Chem. Phys.* **16,** 21225–21229 (2014).
11. Ryu, H. S. *et al.* Self-discharge characteristics of lithium/sulfur batteries using TEGDME liquid electrolyte. *Electrochim. Acta* **52,** 1563–1566 (2006).
12. Mikhaylik Y. V. inventor; Sion Power Corp., assignee. Electrolytes for lithium sulfur cells. United States patent US 7,354,680. 2008 Apr 8.
13. Aurbach, D. *et al.* On the surface chemical aspects of very high energy density, rechargeable Li-sulfur batteries. *J. Electrochem. Soc.* **156,** A694–A702 (2009).
14. Chung, W. J. *et al.* The use of elemental sulfur as an alternative feedstock for polymeric materials. *Nat. Chem.* **5,** 518–524 (2013).
15. Li, Z. *et al.* A highly ordered meso@microporous carbon-supported sulfur@smaller sulfur core-shell structured cathode for Li-S batteries. *ACS Nano* **8,** 9295–9303 (2014).
16. Zhao, Y., Wu, W., Li, J., Xu, Z. & Guan, L. Encapsulating MWNTs into hollow porous carbon nanotubes: a tube-in-tube carbon nanostructure for high-performance lithium-sulfur batteries. *Adv. Mater.* **26,** 5113–5118 (2014).
17. Wang, Z.-L., Xu, D., Xu, J.-J. & Zhang, X.-B. Oxygen electrocatalysts in metal-air batteries: from aqueous to nonaqueous electrolytes. *Chem. Soc. Rev.* **43,** 7746–7786 (2014).
18. Qiu, Y. *et al.* High-rate, ultralong cycle-life lithium/sulfur batteries enabled by nitrogen-doped graphene. *Nano Lett.* **14,** 4821–4827 (2014).

19. Manthiram, A., Fu, Y. & Su, Y.-S. Challenges and prospects of lithium-sulfur batteries. *Acc. Chem. Res.* **46,** 1125–1134 (2013).
20. Liang, X. *et al.* Improved cycling performances of lithium sulfur batteries with $LiNO_3$-modified electrolyte. *J. Power Sources* **196,** 9839–9843 (2011).
21. Jayaprakash, N., Shen, J., Moganty, S. S., Corona, A. & Archer, L. A. Porous hollow carbon@sulfur composites for high-power lithium-sulfur batteries. *Angew. Chem. Int. Ed.* **50,** 5904–5908 (2011).
22. Seh, Z. W. *et al.* Sulphur-TiO_2 yolk-shell nanoarchitecture with internal void space for long-cycle lithium-sulphur batteries. *Nat. Commun.* **4,** 2327 (2013).
23. Chen, R. *et al.* Graphene-based three-dimensional hierarchical sandwich-type architecture for high-performance Li/S batteries. *Nano Lett.* **13,** 4642–4649 (2013).
24. Yang, Y., Zheng, G. & Cui, Y. Nanostructured sulfur cathodes. *Chem. Soc. Rev.* **42,** 3018–3032 (2013).
25. Evers, S. & Nazar, L. F. New approaches for high energy density lithium-sulfur battery cathodes. *Acc. Chem. Res.* **46,** 1135–1143 (2013).
26. Xin, S. *et al.* Smaller sulfur molecules promise better lithium-sulfur batteries. *J. Am. Chem. Soc.* **134,** 18510–18513 (2012).
27. Xu, R., Li, J. C. M., Lu, J., Amine, K. & Belharouak, I. Demonstration of highly efficient lithium-sulfur batteries. *J. Mater. Chem. A* **3,** 4170–4179 (2015).
28. Zhang, S. S. Role of $LiNO_3$ in rechargeable lithium/sulfur battery. *Electrochim. Acta* **70,** 344–348 (2012).
29. Mikhaylik, Y. V. & Akridge, J. R. Polysulfide shuttle study in the Li/S battery system. *J. Electrochem. Soc.* **151,** A1969–A1976 (2004).
30. Zhang, S. S. Improved Cyclability of Liquid Electrolyte Lithium/Sulfur Batteries by Optimizing Electrolyte/Sulfur Ratio. *Energies* **5,** 5190–5197 (2012).
31. Zhang, S. S. Effect of discharge cutoff voltage on reversibility of lithium/sulfur batteries with $LiNO_3$-contained electrolyte. *J. Electrochem. Soc.* **159,** A920–A923 (2012).
32. Zhang, S. S. A new finding on the role of $LiNO_3$ in lithium-sulfur battery. *J. Power Sources* **322,** 99–105 (2016).
33. Diao, Y., Xie, K., Xiong, S. & Hong, X. Analysis of polysulfide dissolved in electrolyte in discharge-charge process of Li-S battery. *J. Electrochem. Soc.* **159,** A421–A425 (2012).
34. Kawase, A., Shirai, S., Yamoto, Y., Arakawa, R. & Takata, T. Electrochemical reactions of lithium–sulfur batteries: an analytical study using the organic conversion technique. *Phys. Chem. Chem. Phys.* **16,** 9344–9350 (2014).
35. Wang, B., Alhassan, S. M. & Pantelides, S. T. Formation of large polysulfide complexes during the lithium-sulfur battery discharge. *Phys. Rev. Appl.* **2,** 034004 (2014).
36. Cheon, S.-E. *et al.* Rechargeable Lithium Sulfur Battery I. Structural Change of Sulfur Cathode During Discharge and Charge. *J. Electrochem. Soc.* **150,** A796–A799 (2003).
37. Akridge, J. R., Mikhaylik, Y. V. & White, N. Li/S fundamental chemistry and application to high-performance rechargeable batteries. *Solid State Ionics* **175,** 243–245 (2004).
38. Rosenman, A. *et al.* The effects of interactions and reduction products of $LiNO_3$, the anti-shuttle agent, in Li-S battery system. *J. Electrochem. Soc.* **162,** A470–A473 (2015).
39. Li, L. *et al.* Enhanced cycling stability of lithium sulfur batteries using sulfur polyaniline-graphene nanoribbon composite cathodes. *ACS Appl. Mater. Interfaces* **6**, 15033–15039 (2014).
40. Zhang, B. *et al.* Novel hierarchically porous carbon materials obtained from natural biopolymer as host matrixes for lithium-sulfur battery applications. *ACS Appl. Mater. Interfaces* **6**, 13174–13182 (2014).
41. Zhou, W., Yu, Y., Chen, H., DiSalvo, F. J. & Abruna, H. D. Yolk-shell structure of polyaniline-coated sulfur for lithium-sulfur batteries. *J. Am. Chem. Soc.* **135,** 16736–16743 (2013).
42. Pang, Q., Kundu, D., Cuisinier, M. & Nazar, L. F. Surface-enhanced redox chemistry of polysulphides on a metallic and polar host for lithium-sulphur batteries. *Nat. Commun.* **5,** 5759 (2014).
43. Tao, X. *et al.* Strong sulfur binding with conducting magneli-phase Ti_nO_{2n-1} nanomaterials for improving lithium-sulfur batteries. *Nano Lett.* **14,** 5288–5294 (2014).
44. Li, Z., Zhang, J. & Lou, X. W. Hollow carbon nanofibers filled with MnO_2 nanosheets as efficient sulfur hosts for lithium-sulfur batteries. *Angew. Chem. Int. Ed.* **54,** 12886–12890 (2015).
45. Wan, C., Wu, W., Wu, C., Xu, J. & Guan, L. A layered porous ZrO_2/RGO composite as sulfur host for lithium-sulfur batteries. *RSC Adv.* **5,** 5102–5106 (2015).
46. Sun, F. *et al.* A high-rate lithium-sulfur battery assisted by nitrogen-enriched mesoporous carbons decorated with ultrafine La_2O_3 nanoparticles. *J. Mater. Chem. A* **1,** 13283–13289 (2013).
47. F1an, Q., Liu, W., Weng, Z., Sun, Y. & Wang, H. Ternary hybrid material for high-performance lithium-sulfur battery. *J. Am. Chem. Soc.* **137,** 12946–12953 (2015).
48. Jiang, J. *et al.* Encapsulation of sulfur with thin-layered nickel-based hydroxides for long-cyclic lithium-sulfur cells. *Nat. Commun.* **6,** 8622 (2015).
49. Over, H. *et al.* Atomic-scale structure and catalytic reactivity of the RuO_2(110) surface. *Science* **287,** 1474–1476 (2000).
50. Kulisch, J., Sommer, H., Brezesinski, T. & Janek, J. Simple cathode design for Li-S batteries: cell performance and mechanistic insights by in operando X-ray diffraction. *Phys. Chem. Chem. Phys.* **16,** 18765–18771 (2014).
51. Chai, J.-D. & Head-Gordon, M. Long-range corrected hybrid density functionals with damped atom-atom dispersion corrections. *Phys. Chem. Chem. Phys.* **10,** 6615–6620 (2008).
52. Gaussian 09, Revision E.01, Frisch, M. J. *et al.* Gaussian, Inc., Wallingford CT, 2009.
53. Grimme, S. Semiempirical GGA-type density functional constructed with a long-range dispersion correction. *J. Comput. Chem.* **27,** 1787–1799 (2006).
54. Hehre, W. J., Ditchfie, R. & Pople, J. A. Self-consistent molecular-orbital methods. 12. Further extensions of gaussian-type basis sets for use in molecular-orbital studies of organic-molecules. *J. Chem. Phys.* **56,** 2257–2261 (1972).
55. Dill, J. D. & Pople, J. A. Self-consistent molecular-orbital methods. 15. Extended gaussian-type basis sets for lithium, beryllium, and boron. *J. Chem. Phys.* **62,** 2921–2923 (1975).
56. Francl, M. M. *et al.* Self-consistent molecular-orbital methods. 23. A polarization-type basis set for 2nd-row elements. *J. Chem. Phys.* **77,** 3654–3665 (1982).
57. Miertus, S., Scrocco, E. & Tomasi, J. Electrostatic Interaction of a Solute with a Continuum. A Direct Utilization of ab Initio Molecular Potentials for the Prevision of Solvent Effects. *Chem. Phys.* **55,** 117–129 (1981).

Acknowledgements

This work was partially supported by a core research grant of the Institute of Materials Research and Engineering (IMRE/14-1C0243), and grants under Advanced Energy Storage Research Program of Science and Engineering Research Council (Award numbers: 1229904044 & 1229904045), A*STAR (Agency for Science, Technology and Research), Singapore. N.D. thanks L. Mechthild of University College London and E. Alter of University of Waterloo for their suggestions in manuscript preparation.

Author Contributions

Y.Z., Z.L., T.S.A.H. and N.D. conceived and designed the experiments. N.D., L.Z., C.Z., D.G., J.Y., S.W.C. and A.Y. synthesized the materials and performed the battery test. M.-F.N. and M.B.S. carried out the calculations. N.D. and Y.Z. analyzed the data and wrote the manuscript. All authors contributed to the discussions and revisions of the manuscript.

Additional Information

Supplementary information accompanies this paper at http://www.nature.com/srep

Competing financial interests: The authors declare no competing financial interests.

How to cite this article: Ding, N. *et al.* Building better lithium-sulfur batteries: from $LiNO_3$ to solid oxide catalyst. *Sci. Rep.* **6**, 33154; doi: 10.1038/srep33154 (2016).